59L.0 IN-SITU VISUALIZATION OF MICROSTRUCTURE EVOLUTION IN METALLIC ALLOYS UNDER ADDITIVE MANUFACTURING CONDITIONS

Oliver Hesmondhalgh (Mines)
Faculty: Amy Clarke (Mines)
Industrial Mentor: Joe McKeown (LLNL)
Other Partners: Gus Becker (Mines), Brian Rodgers (Mines), Alec Saville (Mines), Alain Karma (Northeastern University)

This project initiated in Fall 2021 and is supported by the United States Department of Energy Office of Science. The research performed during this project will serve as the basis for a Ph.D. thesis program for Oliver Hesmondhalgh.

59L.1 Project Overview and Industrial Relevance

Significant advances over the past two decades in metallic additive manufacturing (AM), such as lower cost reliable industrial lasers, inexpensive high-performance computing hardware and software, and metal powder feedstock technology, have enabled it to become a state-of-the-art processing method [59L.1]. In contrast to conventional techniques, AM provides benefits in the production of complex geometries, weight reduction, short lead time, waste reduction, and energy consumption [59L.2]. While certain applications have reached levels of fully certified production, AM is currently limited to low-risk applications due to issues of porosity, surface roughness, cracking and delamination, residual stresses, and uncontrollable microstructural characteristics. A more thorough understanding of the processing path and microstructure and defect development during rapid solidification is required to yield defect-free, structurally-sound, and reliable AM parts.

This project will develop a fundamental understanding of microstructure development under AM conditions by experiments and modeling, as well as develop an understanding of the origins of grain refinement under these conditions. Microstructure prediction and control, in addition to insights into alloy design for AM processes, will aid in the advancement of AM to a wider range of applications. In-situ imaging of aluminum (Al) alloys during simulated AM with Dynamic Transmission Electron Microscopy (DTEM) performed at LLNL and at the Advanced Photon Source (APS) at Argonne National Lab (ANL), followed by ex-situ characterization of these alloys, will allow for the development of AM processes to produce parts with desired structure and properties. Phase field modeling of rapid solidification dynamics will be informed by and compared to novel experimental results obtained at unprecedented length and time scales. In addition, grain refinement in novel Ti alloys will be explore under AM conditions.

59L.2 Previous Work

59L.2.1 Literature Review of Rapidly Solidified Al-Ge

The advent of rapid solidification processing (RSP) has introduced novel microstructures and metastable phases, due to the restricted time for kinetic processes to form stable, faceted phases. The Al-Ge system has been found to form multiple metastable phases, which have been well characterized in preexisting literature [59L.3-6]. That said, the sensitivity of these metastable phases to solidification conditions, such as cooling rate, local undercooling, and solutal conditions, have not been thoroughly investigated. Hexagonal, orthorhombic, monoclinic, and rhombohedral metastable phases have been observed as a product of rapid solidification in Al-Ge alloys [59L.3-10]. These metastable phases do not form metastable equilibrium with each other or the equilibrium β-Ge phase, but only the equilibrium α-Al phase [59L.3, 59L.7]. While the identification of competitive growth conditions of primary phases exists, little work has been done to consider competitive growth between secondary metastable and equilibrium phases [59L.6, 59L.9].

59L.2.2 Experimental DTEM of Al-Ge and Al-Si

DTEM at LLNL was used to capture the rapid solidification dynamics of Al-Ge and Al-Si melt pools of varying compositions. This also allows for in-situ observations of phase and microstructure development at nanosecond temporal and nanometer spatial resolutions. Using this technique, a more exact correlation can be made between solidification conditions and microstructural development, particularly the solidification pathway of metastable phases

in the case of Al-Ge alloys. These links can be used to understand the fundamental mechanisms determining the microstructure selection under additive manufacturing conditions, as well as inform solidification models.

Thin film samples were sputter deposited onto 50 nm thick SiN_x substrates containing a 0.5 mm square window. The compositions of Al-Ge samples are provided in **Table 59L.1** and were pursued to explore the proposed metastable monoclinic phase field seen in **Figure 59L.1** [59L.3].

Al-Si alloys were investigated to study grain competition at high solidification velocities. These results will be compared to state-of-the-art phase-field model predictions by Karma et al. The compositions of Al-Si samples are also provided in **Table 59L.1**. Both hypo- and hyper-eutectic alloy compositions were examined. Nine images of each sample were taken with a 50 nm electron beam pulse and an interframe spacing of 5 µs for the Al-Ge samples and 2 µs for the Al-Si samples. Post-mortem analysis was done using an FEI Talos transmission electron microscope (TEM), employing scanning transmission electron microscopy (STEM) and energy dispersive spectroscopy (EDS) for chemical analysis.

59L.3 Recent Progress

59L.3.1 Processing of Al-Si DTEM Data

The nine images collected for various Al-Si samples were manually analyzed to estimate solidification velocities to inform phase field modeling of rapid solidification dynamics. Image analysis softwares Avizo and imageJ were used successively to track the major and minor axes of each melt pool for each image. In Avizo, a non-local means filter was applied to a set of nine images to denoise the data (**Figure 59L.2A**). The melt pools were then individually segmented from the solidified portions of the sample using an adaptive threshold tool, converted to an 8-bit signed file, and imported to imageJ (**Figure 59L.2B**). A scale was found to be 5.79 pixels/µm in imageJ for a reference image taken at 120x magnification. The segmented portions of the image from Avizo were then selected using a threshold in imageJ, and the Analyze Particles tool was used to acquire the major and minor axes of the melt pools (**Figure 59L.2C**). These measurements were used to inform the change in distance of the melt pool interface, which was divided by the interframe spacing to estimate the solidification velocities of the minor and major axes. The average solidification velocity of each sample was determined to be the average of the major axis and minor axis velocities (**Table 59L.2**). The resulting manual estimates of melt pool solidification velocities were then compared and validated with an automated estimation process developed by Gus Becker (Mines). These results were used to create time-resolved, nanoscale crystallographic maps and grain evolution from ASTAR data.

59L.3.2 Preliminary Analysis of Al-Ge Data

Post-mortem STEM and EDS data allowed for the determination of resulting phases and microstructures of samples with varying compositions after RSP. For samples with low Ge concentrations (~46 at. % Ge), metastable monoclinic (M) phase dendrites formed, surrounded by a monoclinic plus α-Al metastable eutectic. Some primary β particles were also observed (**Figure 59L.3A**). Samples with ~58 at. % Ge resulted in fine β particles near the edges of the melt pools and coarser β particles near the centers of the melt pools. The β particles were sometimes surrounded by Al-rich α phase dendrites near the edges of the melt pool, with M+α metastable eutectic near the centers of the melt pool (**Figure 59L.3B**). In samples with ~63-66 at. % Ge, primary β particles formed finely near the edges and coarsely near the centers of the melt pools. Al-rich dendrites were sometimes only present at the edges of the melt pools, with an unidentified eutectic microconstituent near the centers of the melt pools (**Figure 59L.3C**). Al-rich dendrites were sometimes seen throughout the entire melt pool, from the edges to the centers (**Figure 59L.3D**). It is unknown if eutectic present at the centers of the melt pools in **Figure 59L.3C** is comprised of the equilibrium α+β phases, or the metastable M+α phases. Samples with high Ge contents (~70-76 at. % Ge) did not appreciably form Al-rich α dendrites, but showed large primary β phase particles surrounded by an unidentified eutectic (**Figure 59L.3E**). Current work suggests the competitive growth between the primary β-Ge with equilibrium and/or metastable eutectic with α-Al is due to the local compositions present within the melt pool during solidification. Namely, the volume fraction of primary β phase particles, which is dependent on the Ge concentration, affects local compositions by rejecting Al solute.

59L.4 Plans for Next Reporting Period

Upcoming work will focus on further analyses of the rapidly solidified Al-Ge samples. Training on the FEI Talos TEM with ASTAR capabilities at Mines will also be pursued, which will aid in further evaluations of Al-Ge and Al-Si microstructures, as well as future alloys and phenomena of interest.

- Measurements of eutectic fractions in Al-Ge samples by image analysis techniques.
- Complete training on FEI Talos with ASTAR capabilities at Mines.
- Summarize results on Al-Ge microstructure development in DTEM samples and further characterization, if needed, and prepare a peer-reviewed journal manuscript.
- Complete training on the creation of focused ion beam (FIB) foils for TEM analysis in anticipation of future work.
- Aid in Al-Si microstructure characterization produced by DTEM to inform modeling and further understanding of competitive grain growth during rapid solidification.
- Study novel Ti alloys with grain refinement potential under additive manufacturing conditions.

59L.5 References

[59L.1] T. DebRoy, H.L. Wei, J.S. Zuback, T. Mukherjee, J.W. Elmer, J.O. Milewski, A.M. Beese, A. Wilson-Heid, A. De, W. Zhang. Additive Manufacturing of Metallic Components – Process, Structure, and Properties, Progress in Materials Science. 92 (2018) 112-224.

[59L.2] C. Körner. Additive Manufacturing of Metallic Components by Selective Electron Beam Melting – A Review, International Materials Reviews. 61 (2016) 361-377.

[59L.3] T. Laoui, M.J. Kaufman. Nonequilibrium Behavior in the Al-Ge Alloy System: Insights into the Metastable Phase Diagram, Metallurgical Transactions A. 22 (1991) 2141-2152.

[59L.4] S.N. Ojha, K. Chattopadhyay, P. Ramachandra Rao. Phase Transformations and Metastable Phase Equilibria in Al-Ge Alloy, Materials Science and Engineering. 73 (1985) 177-183.

[59L.5] S. Srikanth, D. Sanyal, P Ramachandra Rao. A Re-Evanuation of the Al-Ge System, Calphad. 20 (1996) 312-332.

[59L.6] T. Laoui, M.J. Kaufman. Metastable Phase Equilibria in Faceted-Nonfaceted Systems, Scripta Metallurgica et Materialia. 30 (1994) 1563-1567.

[59L.7] M.J. Kaufman, J.E. Cunningham, H.L. Fraser. Metastable Phase Production and Transformation in Al-Ge Alloy Films by Rapid Crystallization and Annealing Treatments, Acta Metallurgica. 35 (1987) 1181-1192.

[59L.8] M.J. Kaufman, H.L. Fraser. Analysis of In-Situ Rapid Solidification of Submicron Al-Ge Eutectic Powders Using Transmission Electron Microscopy, Metallurgical Transactiona A. 14 (1983) 623-633.

[59L.9] M.J. Kaufman, H.L. Fraser. Characterization of Metastable Crystalline Phases in the Al-Ge Alloy System, Acta Metallurgica. 33 (1985) 191-203.

[59L.10] S.N. Ohja. Metastable Phase Formation During Solidification of Undercooled Melt, Materials Science and Engineering. A304 (2001) 114-118.

59L.6 Figures and Tables

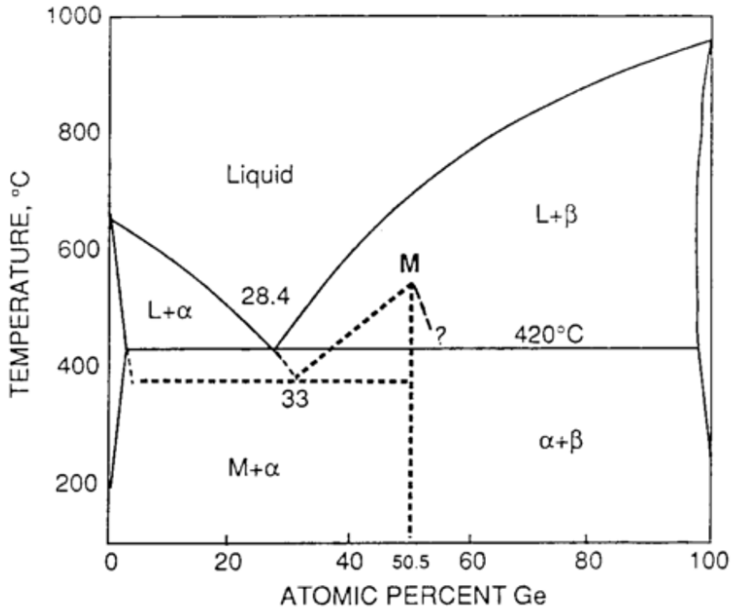

Figure 59L.1: Proposed metastable phase diagram for the monoclinic (M) phase superimposed on the equilibrium Al-Ge phase diagram [59L.3].

Table 59L.1: Nominal and real compositions of Al-Ge and Al-Si sputter deposited thin film samples.

System	Nominal Composition [at. % Ge, Si]	Real Composition [at. % Ge, Si]
Al-Ge	33	46
	40	58
	43	63
	45	60-63
	48	63-69
	53	70-76
Al-Si	1	1
	3	3.1
	6	6.2
	9	9.3
	12	12
	15	15

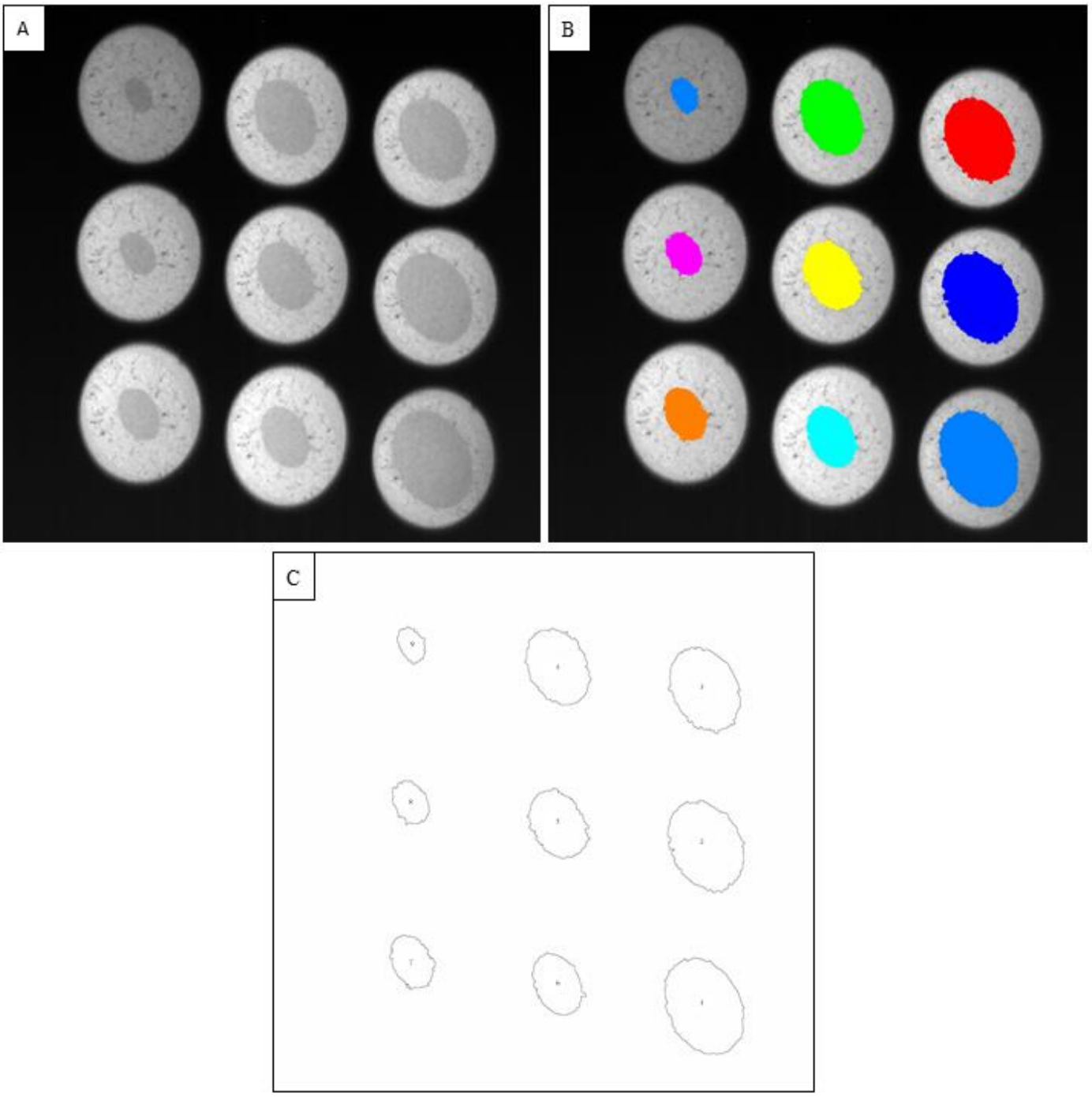

Figure 59L.2: In-situ images collected using DTEM for an Al-3Si sample. A) Denoising of the images by applying a non-local means filter in Avizo. B) Individually segmented melt pools using an adaptive threshold tool in Avizo. C) Outlines of the melt pools on which the Analyze Particles tool in imageJ was used to calculate the major and minor axes of each melt pool. The melt pools are labeled in numerical order from first image taken after the laser hit (1) to last image taken after the laser hit (9).

Table 59L.2: Average solidification velocity determined through manual image analysis of Al-Si DTEM images.

Nominal Sample Composition [at. %]	Laser Shot Energy (µJ)	Average Solidification Velocity (m/s)
Al-3Si	3.22	1.85
Al-3Si	3.17	1.99
Al-6Si	2.34	1.33
Al-9Si	1.78	1.29
Al-12Si	2.05	1.14
Al-15Si	1.57	0.803

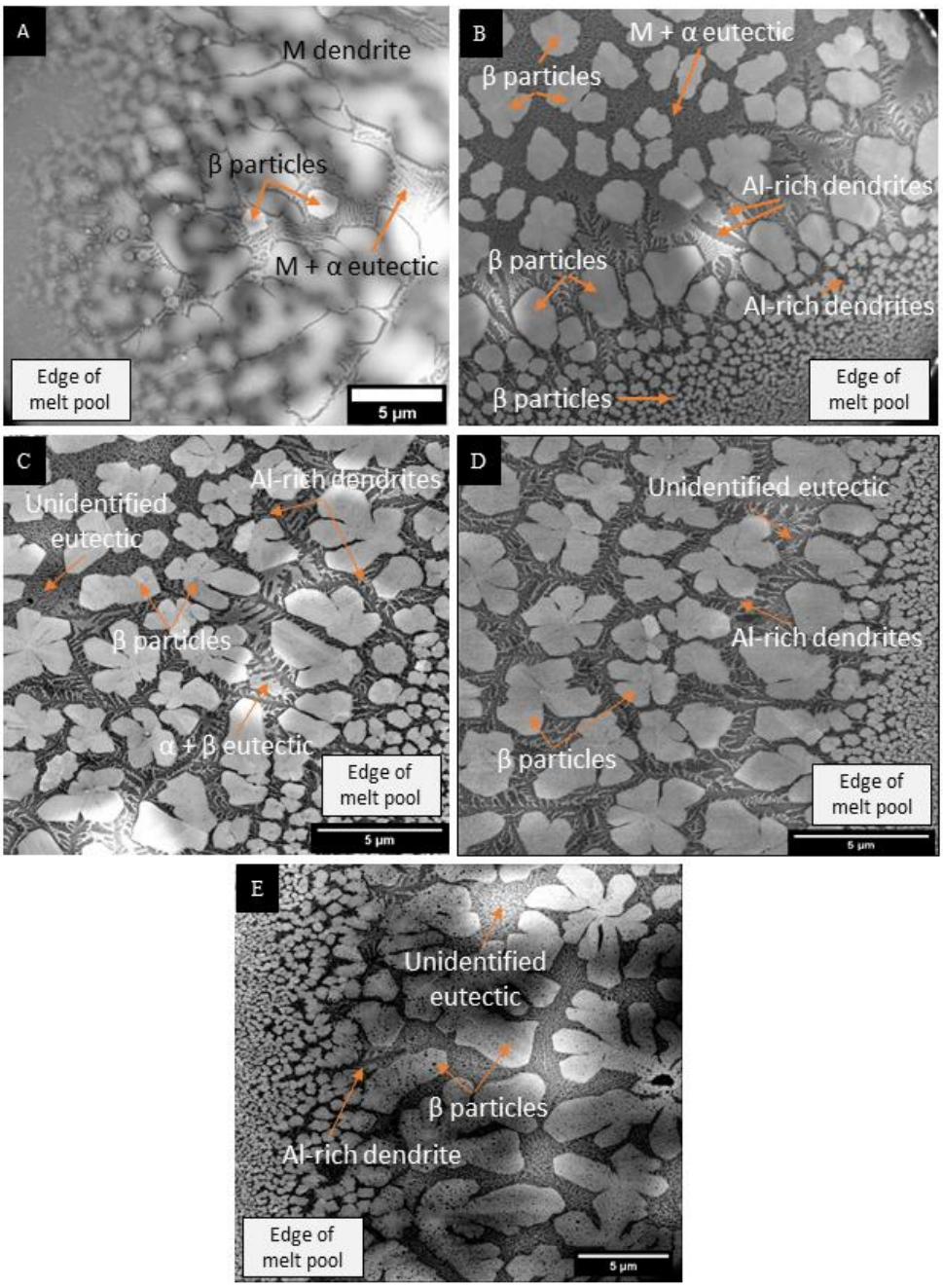

Figure 59L.3: HAADF TEM images of melt pools from Al-Ge DTEM foil samples of differing compositions. A) 46 at. % Ge showing large M phase dendrites surrounded by the metastable M+α eutectic, with primary β particles between the dendrites. B) 58 at. % Ge with fine β particles near the edge of the melt pool and coarser β particles near the center of the melt pool. The β particles are surrounded by Al-rich dendrites near the edge of the melt pool, but M+α metastable eutectic near the center of the melt pool. C) 63-66 at. % Ge with fine primary β particles near the edge of the melt pool and coarse β particles near the center of the melt pool. Al-rich α phase dendrites only at the edge of the melt pool with an unidentified eutectic phase near the center of the melt pool. D) 63-66 at. % Ge with fine primary β particles near the edge of the melt pool and coarse β particles near the center of the melt pool. Al-rich α phase dendrites are shown throughout the entire melt pool surrounded by an unidentified eutectic. E) 70-76 at. % Ge with large primary β particles surrounded by an unidentified eutectic, with minimal Al-rich α phase dendrites.